Catalysis Today 175 (2011) 625–630

Contents lists available at ScienceDirect

Catalysis Today

journal homepage: www.elsevier.com/locate/cattod

Theoretical and experimental study on the deactivation of V_2O_5 based catalyst by lead for selective catalytic reduction of nitric oxides

Xiang Gao*, Xue-sen Du, Yin-cheng Fu, Jian-hong Mao, Zhong-yang Luo, Ming-jiang Ni, Ke-fa Cen

State Key Laboratory of Clean Energy Utilization, Zhejiang University, No. 38 Zheda Road, Hangzhou 310027, Zhejiang PRC, PR China

ARTICLE INFO

Article history:
Received 11 October 2010
Received in revised form 18 May 2011
Accepted 24 May 2011
Available online 19 July 2011

Keywords:
Selective catalytic reduction
Deactivation
Lead
Density functional theory
V_2O_5

ABSTRACT

A combination of theoretical and experimental methods, including DFT calculation, BET, Raman spectroscopy, NH_3-TPD, H_2-TPR and XPS, has been used to elucidate the mechanism of lead deactivating effect on the V_2O_5 based SCR catalyst. The theoretical calculations have shown that the doping of lead atom will cause the great change of the surface electronic property. Each lead atom will influence two active sites, resulting in the decrease of the acid formability and reducibility of the catalyst surface. The NH_3-TPD and H_2-TPR experiments have shown the decrease of acid site amount and reducibility, which is in accordance with the calculation result. The BET result has also shown the physical influence caused by the doping of lead compound. The NO conversion experiment has confirmed the deactivation effect of lead on the V_2O_5 based catalyst.

1. Introduction

The selective catalytic reduction (SCR) of nitric oxides has been widely used to remove NOx emitted from stationary sources and vehicles [1]. V_2O_5 based catalyst has been regarded as an efficient SCR catalyst and successfully applied for decades.

During the industrial application of V_2O_5 based catalyst, catalyst deactivation has drawn much attention. Alkaline metals, such as alkali metals (K, Na), alkaline earth metals (Ca) and some heavy metals (Pb, As) are all responsible for catalysis deactivation, as reported by many researchers [2–13]. The influences of alkali and alkaline earth metals on the SCR catalyst have been widely reported [2–10]. Lots of experimental and theoretical methods, including BET, FTIR, XPS, NH_3-TPD, H_2-TPR and DFT calculations, have been employed to reveal the mechanism of catalyst deactivation by alkali metals. The results showed that alkali metals, such as K and Na, strongly affect the acidity and surface reducibility, thus reducing the activity of the catalyst [2–10].

Lead (Pb) is one of the main poisonous elements in the flue gas of power plants and municipal waste incinerator [11]. Khodayari and Odenbrand [12] found a strong accumulation effect of lead on the SCR catalyst and the lead concentration reached 3350 ppm after running for 1908 h in a municipal waste incinerator. Therefore, it is important to reveal the deactivating mechanism of V_2O_5 based catalyst by lead. The subsequent research by Khodayari and Odenbrand [12] suggested that Pb will significantly decrease the NH_3 chemisorption, thus resulting in the deactivation of SCR catalyst. Chen et al. [11] also found the deactivation of lead and suggested that the poisoning strength of Pb was between the two serious poisoning elements K and Na. Unlike alkali metals, the deactivation mechanism of lead has been rarely reported.

In this work, the deactivation mechanism of Pb on V_2O_5 based SCR catalyst was studied. DFT calculations were carried out to elucidate the atomic interaction of the Pb with the catalyst surface. Electrostatic potential (ESP) analysis was firstly performed to illustrate why Pb will influence the surface acidity of the V_2O_5 based catalyst. Meanwhile, BET, NH_3 TPD, H_2-TPR and XPS were performed to experimentally reveal the deactivation effect of Pb compound.

2. Experimental

2.1. Computational details

All density functional theory (DFT) calculations were performed with Gaussian 03 [14] code using the gradient corrected Becke's [15,16] three-parameter hybrid exchange functional in combination with the correlation functional of Lee et al. [17] (B3LYP). LanL2DZ basis was used for all these models. Each stationary structure was confirmed as a minimum-energy structure from the calculated vibrational frequencies. The vibrational frequencies obtained by frequency calculations were scaled by 0.9607 [18].

* Corresponding author. Tel.: +86 135 05711887; fax: +86 571 87951616.
E-mail addresses: xgao1@zju.edu.cn (X. Gao), dxs_1987@zju.edu.cn (X.-s. Du), fyc_hust_zju@zju.edu.cn (Y.-c. Fu).

0920-5861/$ – see front matter © 2011 Elsevier B.V. All rights reserved.
doi:10.1016/j.cattod.2011.05.025

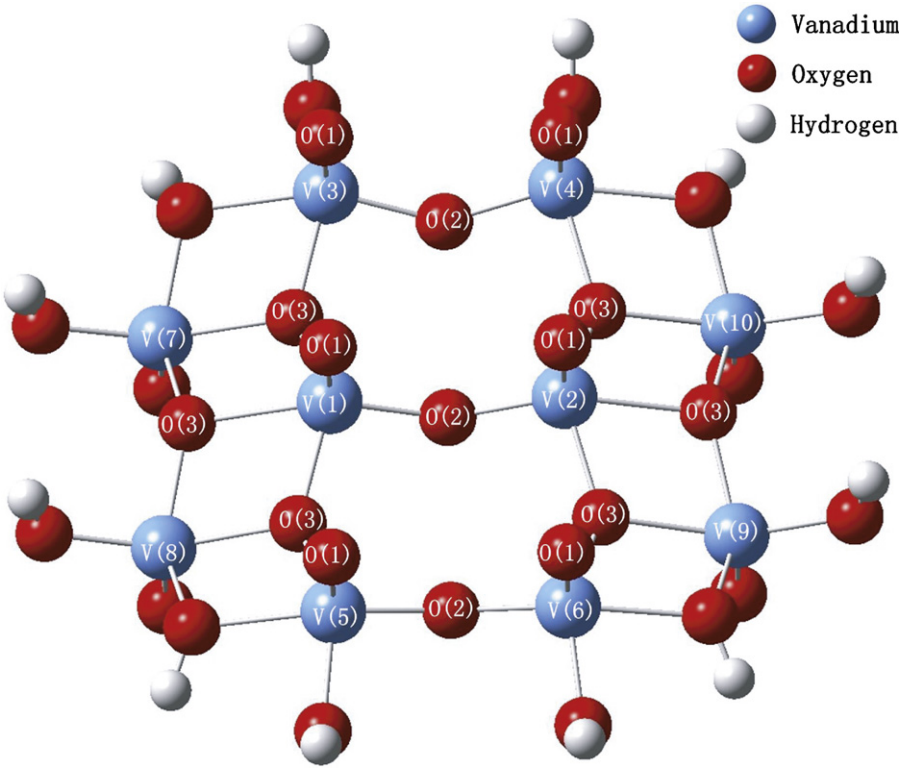

Fig. 1. The stationary structure of $V_{10}O_{39}H_{12}$ model.

In this study, a $V_{10}O_{39}H_{12}$ model (Fig. 1), which is thought to be a proper model to represent the geometric and electronic structure of vanadium pentoxide [19–24], is employed to simulate the V_2O_5 catalyst surface. Fig. 1 was achieved by optimizing a $V_{10}O_{39}H_{12}$ model, which was conducted by taking ten vanadium atoms and 39 bonded oxygen atoms from the (0 1 0) plane of V_2O_5 catalyst. This surface contains three structurally different oxygen sites: vanadyl oxygens coordinated to one vanadium, O(1) and bridging oxygens [O(2) or O(3)] respectively coordinated with two or three vanadium atoms. Charge neutrality was maintained by adding hydrogen atoms to the peripheral oxygen atoms. After optimization, the V–V distances are 339 pm and 354 pm, in good agreement with 346 pm and 361 pm [25]. The deviations are attributed to the different basis employed. The V=O(1), V–O(2), V–O(3) are 158 pm, 176 pm and 1.87–2.12 pm respectively, in agreement with the former computing results [20].

Lead atoms were doped to the center of four O(1) to probe the chemical influence of lead on the V_2O_5 catalyst. The doped systems were also optimized at the B3LYP/LanL2DZ level. Throughout the optimization process, all the vanadium atoms were fixed. Mulliken charge and ESP (electrostatic potential) calculations were conducted to evaluate the electronic property and approachability of H^+ to the O(1) of the models.

2.2. Catalyst preparation

All the experiments were carried out on a V_2O_5/TiO_2 catalyst with V_2O_5 loading of 1 wt% (1V/Ti) prepared by impregnation method. Ammonium metavanadate (NH_4VO_3) precursor was used to impregnate the TiO_2 support (anatase). The mixture was heated at 70 °C in a water bath for 4 h and then dried at 105 °C for 12 h. Afterwards, the catalyst was incinerated at 500 °C in air for 5 h.

The Pb-containing samples were prepared by impregnating the 1V/Ti catalyst with aqueous acetate solution ($Pb(CH_3COO)_2$). Catalyst doping procedure is as follows: impregnated with aqueous acetate solution, heated at 70 °C in a water bath for 4 h, dried at 105 °C for 12 h and incinerated at 500 °C in air for 5 h. The doping concentration of lead was 50 mol% based on vanadium (Pb/V = 0.5).

2.3. NH_3-TPD

The Temperature Programmed Desorption of ammonia (NH_3-TPD) was carried out on an AutoChem II 2920 instrument manufactured by Micromeritics Corporation. NH_3 desorption was detected by a QIC20 mass spectrum instrument provided by Hiden Corporation. The mass number used for monitoring the desorbed NH_3 is $m/e = 17$. Approximately 0.2 g of powder catalyst was first pretreated in a stream of He at 20 mL/min while heating up to 500 °C at 50 °C/min. After a hold time of 30 min, the sample was cooled down to 100 °C and saturated with a 20 mL/min gas mixture of 5% NH_3 in He for 30 min. At the end of the saturation process, the sample was cooled to 50 °C and flushed with pure He at 50 mL/min until the TCD signal was stabilized. The sample was then heated up to 700 °C (ramp 10 °C/min) and the mass spectrum signal of NH_3 desorbed from the catalyst surface was collected.

2.4. H_2-TPR

Hydrogen temperature-programmed reduction (H_2-TPR) was performed in a quartz tube reactor. A H_2/Ar mixture (10 vol.% H_2) with a flow rate of 20 mL/min was used as the reductant. Each sample (100 mg) was placed in the reactor and pre-treated at 500 °C in Helium for 30 min. Subsequently the sample was cooled to room temperature and then the temperature increased to 800 °C at a rate of 10 K/min under 10 vol.% H_2/Ar. The consumption of H_2 was measured by a thermal conductivity detector (TCD).

2.5. Catalytic activity test

The catalytic activity tests for the reduction of NO by NH_3 were carried out in a fixed bed micro-reactor with catalyst samples of

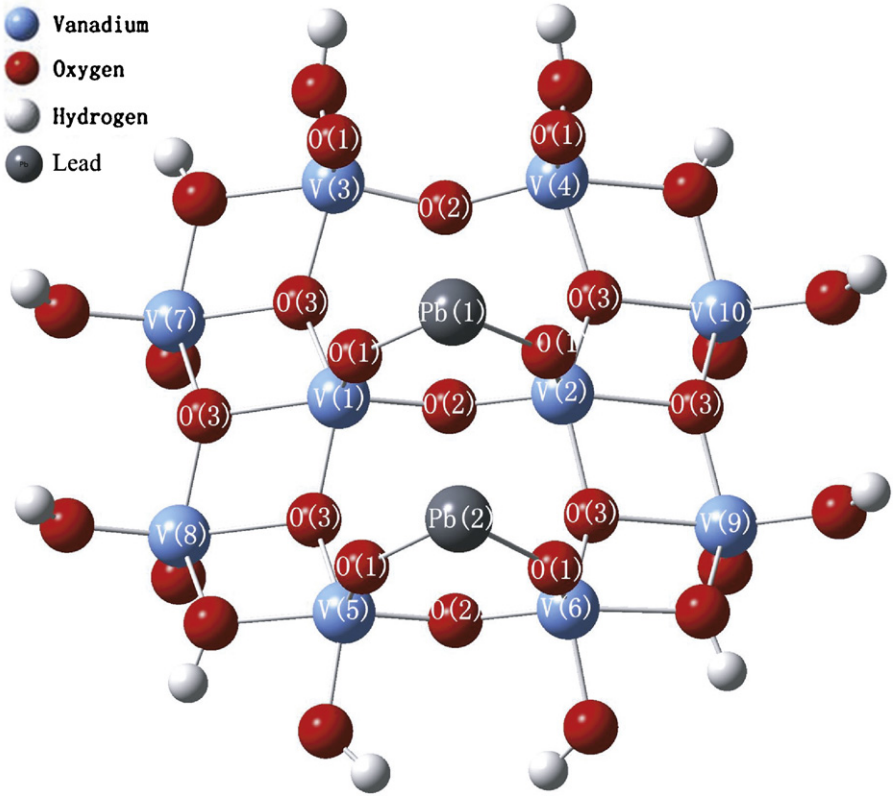

Fig. 2. The stationary structure of Pb-doped catalyst model.

125 mg. The simulated gas for these tests contained 1000 ppm NO, 3 vol.% O_2 and 1000 ppm NH_3 in He. The catalytic reactions were carried out at 0.1 MPa with a total flow rate 0.5 L/min and GHSV = $1.2 \times 10^5\ h^{-1}$ (based on the total bed volume of catalyst samples). The NO concentrations were determined by a Rosemount NGA2000 analyzer. N_2O, NO_2 and NH_3 were detected with infrared methods using a Gasmet analyzer.

2.6. Catalyst characterization

Brunauer–Emmett–Teller (BET) surface area was measured by N_2 adsorption at 77 K using a Quantachrome Autosorb-1 instrument. Raman spectra were run with a single monochromator Renishaw Invia microscope Raman. The powder samples were excited with the 514 nm Ar^+ line; spectral resolution was 2 cm^{-1} and spectrum acquisition consisted of 20 accumulations of 10 s. The XPS spectra were recorded on a Thermo ESCALAB 250 X-ray photoelectron spectrometer using Al Ka ($h\upsilon$ = 1486.6 eV) as a radiation source at 150 W. Binding energies (BE) were measured for Pb and sample charging effects were eliminated by correcting the observed spectra with the C 1s binding energy value of 284.8 eV.

3. Results and discussion

3.1. Theoretical calculations and discussion

Two lead atoms are added onto the surface of the $V_{10}O_{31}H_{12}$ catalyst model and the achieved model was optimized at the B3LYP/LanL2DZ level. The stationary structure of the Pb-doped V_2O_5 catalyst model is shown in Fig. 2. From the calculation results, Pb doping will have a significant influence on the catalyst. As can be seen in Fig. 2, Pb is strongly adsorbed to the middle of two V=O sites. In the optimized model, Pb is coordinated to two O(1) with a bond length of 0.218 nm for O(1)-Pb. Some characteristics of the undoped and doped models are given in Table 1. The Pb doping will cause the extending of the V=O bond. The V(1)=O(1a) bond length in the undoped model is 0.158 nm at the B3LYP/LanL2DZ level, which agrees with the previous calculation results [10]. Doping with Pb will extend the V(1)=O(1a) bond length to 0.166 nm, which decreases the interaction between V and O(1). The frequency calculation results show a great shift of V=O stretching frequency from 1130/1109 cm^{-1} to 909/880 cm^{-1} for Pb-doping.

Mulliken charge calculations were performed to analyze the interactions between the doped Pb and nearby atoms. The doped Pb atoms are positively charged (+0.765), which implies the contribution of the valance electron to nearby O(1) atoms. The Milliken charge of a PbO molecular was also calculated to compare with the Pb in this Pb-doped catalyst. The result shows that Pb in the Pb-doped catalyst model is more positively charged than in the PbO molecular (+0.695). The contribution of the valance electron from Pb to the catalyst will produce electron reorganization on the catalyst surface, which might lead to a change in catalyst reactivity. Lowest unoccupied molecular orbital (LUMO) calculations were carried out to probe the reactivity of the catalyst with nucleophilic species. The results demonstrate an increase of LUMO energy with the doping of Pb, as shown in Table 1. The higher LUMO energies of the doped models indicate the lower activities to nucleophilic species.

Terminal Brønsted acid V-OH is thought to be very important to SCR reaction [25]. Brønsted acid sites can be formed by the dissociation of water molecular [26]. The process begins when a H_2O molecule approaches the V_2O_5 surface. Due to the polarity of the V=O double bond, the H_2O molecule will dissociate into OH^- and H^+, interacting with V and O, respectively. The ionic bonding between OH^- and H^+ will vanish because of the highly charged V and O. This produces the terminal Brønsted acid that serves as the active site for the adsorption and activation of ammonia, V-OH. The approachability of H^+ to the O(1) indicates the formability of termi-

Table 1
Model characters before and after Pb-doped.

Catalyst model	Basis	V(1)=O(1a) bond length	Stretching frequency (V=O)	LUMO energy
V10	Lanl2dz	0.158 nm	1130 cm^{-1}	−0.1686 Hartree
V10pbpb	Lanl2dz	0.166 nm	880 cm^{-1}	−0.1527 Hartree

nal Brønsted acid V-OH. The ESP characteristics were calculated to evaluate the approachability of H^+ to the terminal O for $V_{10}O_{39}H_{12}$ and doped systems to elucidate the Brønsted acid sites changes. The ESP indicates the approachability of a proton from infinity. A positive value of ESP indicates the approach of H^+ from infinity is endothermic, while a negative value implies the opposite. In Fig. 3, ESP contours in the V(1)-V(2)-O(1b)-O(1a) plane (Fig. 1) are given for the undoped and doped models. The undoped catalyst model (Fig. 3A) has a negative-value ESP zone around the two terminal O(1) atoms. Hence, H^+ can easily approach this area and interact with O(1). Afterwards, the terminal Brønsted acid, V-OH, can be readily generated. Doping with Pb will influence the ESP, as can be seen in Fig. 3B. The Pb atom diminishes the negative-ESP zone around the terminal O(1), which reduces the approachability of H^+ to the O(1) atoms. The positive charges (Table 1) of Pb are responsible for the change in ESP. The positively charged Pb will repel the approach of H^+ and increase the energy consumption required for H^+ to approach.

3.2. Experimental results and discussion

N_2 BET was measured to evaluate the physical properties of the samples. The results (Table 2) show that the V_2O_5/TiO_2 catalyst surface area decreases with the doping of PbO. Table 2 has also

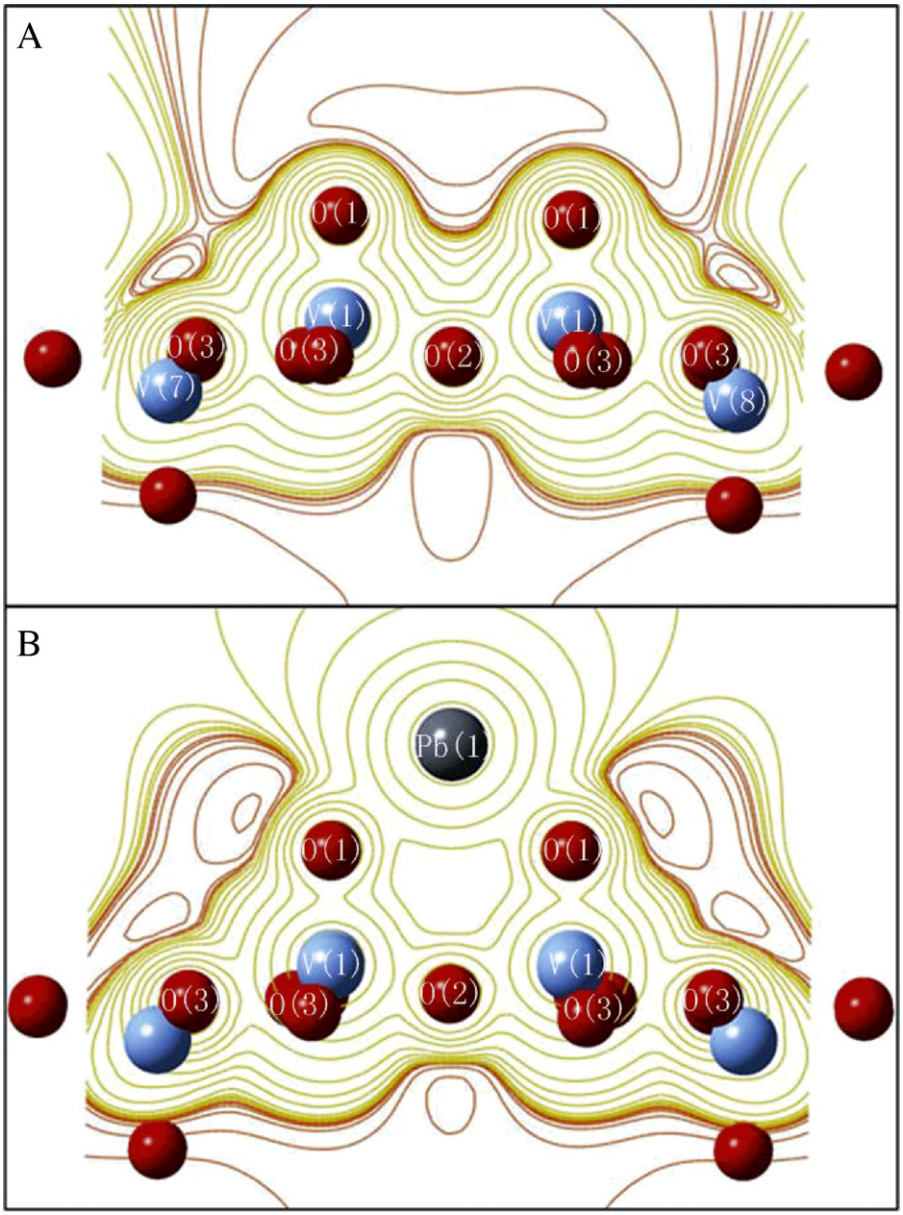

Fig. 3. ESP contours of catalyst models. (A) Undoped and (B) Pb-doped. Red lines indicate negative values; Yellow-green lines indicate positive values. (For interpretation of the references to color in this figure legend, the reader is referred to the web version of the article.)

Table 2
Physical properties of the undoped and Pb-doped catalysts.

Sample	Pb loading (%)	Surface area (m^2/g)	Total pore volume (cm^3/g)	Average pore size (Å)
Undoped	0	98.57	0.3702	146.8
Pb-doped	1.1392	79.14	0.3229	163.2

shown the total pore volume and average pore size of the catalysts. The decrease of the total pore volume indicates that PbO will cover the surface of the catalyst surface and block the pores. The average pore size increases from 146.8 to 163.2 Å, which confirms that PbO will block the smaller pores of the catalyst.

The Raman spectra of the undoped and Pb-doped samples were shown in Fig. 4. The calculated V=O stretching frequencies were also inserted in this figure. The band at 1023 cm^{-1} is attributed to the vibration of the terminal vanadyl group (V=O) [28]. The addition of the Pb to the catalysts induces a red shift (from 1023 to 973 cm^{-1}) of the vibration frequency related to V=O bond. It indicates a weakening of the V=O double bond. The experimental results obtained confirm the red shift of V=O bond stretching and the prediction of V=O bond elongation caused by Pb addition to the catalyst described by modeling.

NH_3-TPD was used to probe the change of surface acidity caused by the PbO doping. Fig. 5 shows the original NH_3-TPD curves from the catalyst samples in the range of 100–600 °C. As can be seen from the figure, the NH_3 desorption of the catalyst shifts to the low-temperature side because of the Pb doping. According to previous results [7], the curves of V_2O_5/TiO_2 catalyst can be treated as two peaks, i.e. weakly chemisorbed NH_3 and strongly chemisorbed NH_3. The weakly chemisorbed NH_3 has a maximum desorption peak at temperatures around 250 °C and strongly chemisorbed NH_3 largely desorbed at around 400 °C, as shown in Fig. 5. The comparison between the results of undoped and Pb-doped sample reveals that both the weakly chemisorbed NH_3 and strongly chemisorbed NH_3 decrease due to the doping of lead compound. This phenomenon can be caused by either the physical covering of PbO on the catalyst surface or chemical interaction between Pb atoms and the active V=O sites. Another noticeable phenomenon is the shift of the desorption curve to lower temperature because of the Pb doping. This confirms that PbO can chemically interact with the active site on the catalyst surface.

The H_2-TPR curves of the undoped and PbO doped catalyst are shown in Fig. 6. Only one H_2 consumption peak at 467 °C has been observed for the undoped sample. The doping of PbO has caused a shifting of the main peak to a high temperature and an arising of a new consumption peak (C). The difference between these two curves indicates the decrease of reducibility of the catalyst at low temperature because of the PbO doping. The arising of the new peak (C) is attributed to the reduction of surface oxygen coordinated to the Pb atoms.

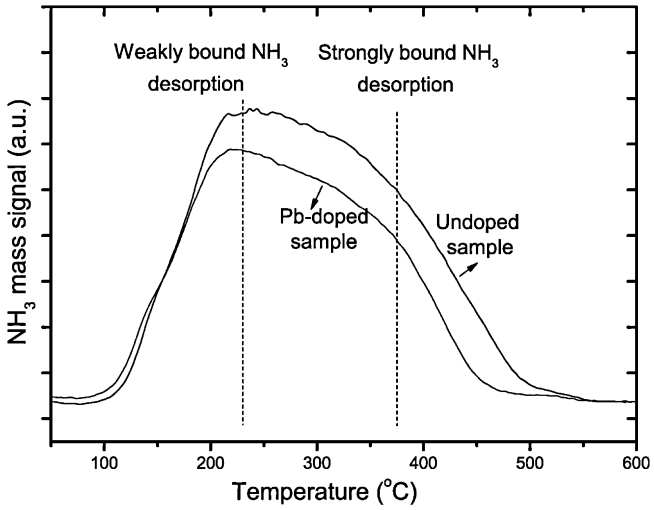

Fig. 5. NH_3-TPD profiles of Undoped and Pb-doped catalyst.

The XPS characterization was also performed for Pb element in the Pb-doped catalyst. As detected, Pb in the catalyst possesses a $4f_{2/5}$ peak at 144.3 ev and a $4f_{2/7}$ peak at 139.5 ev. The traditional molecular Pb has a $4f_{2/7}$ peak at 136.6 ev and PbO has a $4f_{2/7}$ peak at 137.5 ev [27]. Thus the Pb element in our Pb-doped sample is more highly oxidized than that in PbO molecular. This is in accordance with the calculated result that Pb in the Pb-doped catalyst is more positively charged than that in the PbO molecular. This also confirms the electronic interaction between Pb and the catalyst surface.

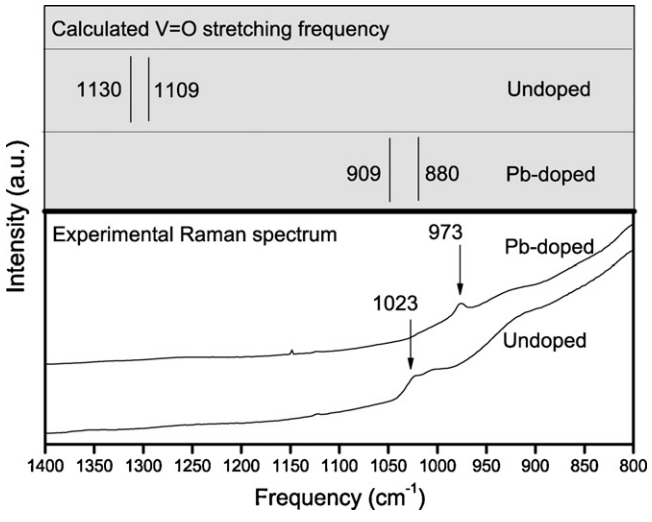

Fig. 4. Calculated and experimental Raman profiles of the undoped and Pb-doped samples.

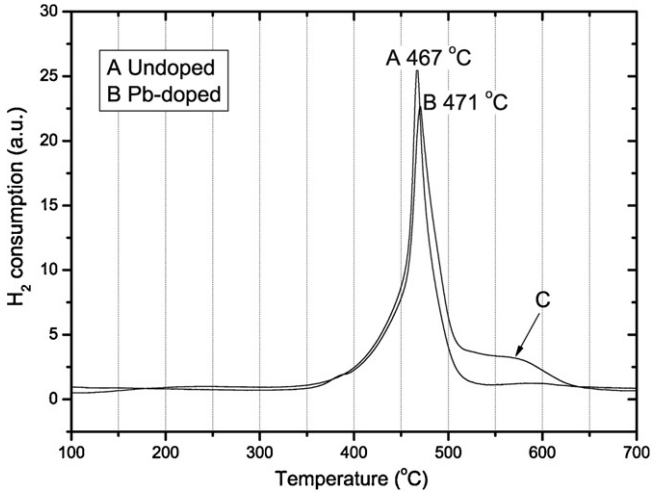

Fig. 6. H_2-TPR profiles of Undoped and Pb-doped catalyst.

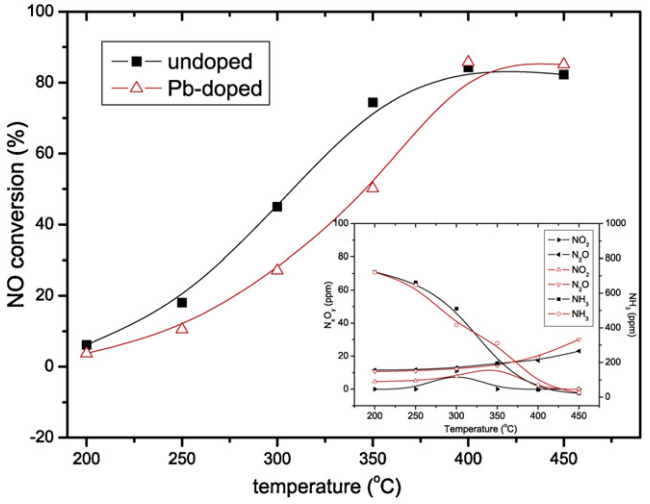

Fig. 7. NO reduction activities of the undoped and Pb-doped catalysts; Outlet NO_2, N_2O and NH_3 concentrations in the inserted figure (solid, black symbol for undoped sample; hollow, red symbol for Pb-doped sample). (For interpretation of the references to color in this figure legend, the reader is referred to the web version of the article.)

Finally, NO reduction experiments were carried out to identify the results discussed above. The results are given in Fig. 7. The NO conversion was reduced by the PbO doping at the temperatures below 400 °C. This phenomenon is in conformity with the results discussed above. The doping of Pb has caused the decrease of surface area, NH_3 adsorption amount and reducibility of the surface as well. Thus, these changes have led to the decrease of NO conversion. The NO_2, N_2O and NH_3 concentrations after reaction are also detected, as shown in the inserted figure of Fig. 7. NO_2 and N_2O were both below 30 ppm at all these temperatures when the inletting NO is 1000 ppm. The calculated results indicted that the selectivity was maintained at a high level (above 97%) for both undoped and Pb-doped samples. The NH_3 concentrations of these two samples showed the similar profiles, which led to the fact that the Pb doping did not enhance the side reactions, such as NH_3 oxidation.

4. Conclusions

Acid sites and the reducibility of the surface are crucial for a V_2O_5 based catalyst in an SCR reaction. DFT calculations and experiments were carried out to probe the influence of Pb on a V_2O_5 based catalyst. The theoretical calculations have shown that the doping of Pb will cause the great change of the surface electronic property. Each Pb atom will influence two active sites, resulting in the weakening of the V=O double bond and the increase of LUMO energy. The calculated Mulliken charge and XPS result have both shown that Pb element in Pb-doped catalyst is more positively charged than in the PbO molecular. This electronic interaction between Pb and the catalyst surface will cause the surface reducibility. Red shifts in the V=O stretching frequency were observed with the Pb doping. The theoretical ESP differences between the undoped and doped models show the decrease of Brønsted acid formability caused by the Pb doping. The NH_3-TPD and H_2-TPR experiments have demonstrated the decrease of acid site amount and surface reducibility, which are in accordance with the calculation results. The BET result has also revealed the physical influence caused by the PbO doping. The deactivation effect of Pb on the V_2O_5 based catalyst was finally confirmed by The NO conversion experiments.

Acknowledgements

We gratefully acknowledge the financial support of the National Natural Science Foundation of China (no. 50776079) and Development of China (863 Program) (no. 2007AA061802).

References

[1] L. Chen, J.H. Li, M.F. Ge, J. Phys. Chem. C 113 (2009) 21177–21184.
[2] T. Shikada, K. Fujimoto, Chem. Lett. (1983) 77–80.
[3] L. Lisi, G. Lasorella, S. Malloggi, G. Russo, Appl. Catal. B 50 (2004) 251–258.
[4] A.L. Kustov, M.Y. Kustova, R. Fehrmann, P. Simonsen, Appl. Catal. B 58 (2005) 97–104.
[5] Y.J. Zheng, A.D. Jensen, J.E. Johnsson, J.R. Thogersen, Appl. Catal. B 83 (2008) 186–194.
[6] J. Due-Hansen, S. Boghosian, A. Kustov, P. Fristrup, G. Tsilomelekis, K. Stahl, C.H. Christensen, R. Fehrmann, J. Catal. 251 (2007) 459–473.
[7] D. Nicosia, I. Czekaj, O. Krocher, Appl. Catal. B 77 (2008) 228–236.
[8] O. Krocher, M. Elsener, Appl. Catal. B 77 (2008) 215–227.
[9] F. Castellino, A.D. Jensen, J.E. Johnsson, R. Fehrmann, Appl. Catal. B 86 (2009) 196–205.
[10] F. Castellino, A.D. Jensen, J.E. Johnsson, R. Fehrmann, Appl. Catal. B 86 (2009) 206–215.
[11] J.P. Chen, M.A. Buzanowski, R.T. Yang, J.E. Cichanowicz, J. Air Waste Manage. Assoc. 40 (1990) 1403–1409.
[12] R. Khodayari, C.U.I. Odenbrand, Ind. Eng. Chem. Res. 37 (1998) 1196–1202.
[13] J.P. Chen, R.T. Yang, J. Catal. 125 (1990) 411–420.
[14] G.W.T.M.J. Frisch, H.B. Schlegel, G.E. Scuseria, M.A. Robb, J.R. Cheeseman, J.A. Montgomery Jr., T. Vreven, K.N. Kudin, J.C. Burant, J.M. Millam, S.S. Iyengar, J. Tomasi, V. Barone, B. Mennucci, M. Cossi, G. Scalmani, N. Rega, G.A. Petersson, H. Nakatsuji, M. Hada, M. Ehara, K. Toyota, R. Fukuda, J. Hasegawa, M. Ishida, T. Nakajima, Y. Honda, O. Kitao, H. Nakai, M. Klene, X. Li, J.E. Knox, H.P. Hratchian, J.B. Cross, C. Adamo, J. Jaramillo, R. Gomperts, R.E. Stratmann, O. Yazyev, A.J. Austin, R. Cammi, C. Pomelli, J.W. Ochterski, P.Y. Ayala, K. Morokuma, G.A. Voth, P. Salvador, J.J. Dannenberg, V.G. Zakrzewski, S. Dapprich, A.D. Daniels, M.C. Strain, O. Farkas, D.K. Malick, A.D. Rabuck, K. Raghavachari, J.B. Foresman, J.V. Ortiz, Q. Cui, A.G. Baboul, S. Clifford, J. Cioslowski, B.B. Stefanov, G. Liu, A. Liashenko, P. Piskorz, I. Komaromi, R.L. Martin, D.J. Fox, T. Keith, M.A. Al-Laham, C.Y. Peng, A. Nanayakkara, M. Challacombe, P.M.W. Gill, B. Johnson, W. Chen, M.W. Wong, C. Gonzalez, J.A. Pople, Gaussian 03, Revision B. 02, Gaussian Inc., Pittsburgh, PA, 2003.
[15] A.D. Becke, Phys. Rev. A 38 (1988) 3098–3100.
[16] A.D. Becke, J. Chem. Phys. 98 (1993) 5648–5652.
[17] C.T. Lee, W.T. Yang, R.G. Parr, Phys. Rev. B 37 (1988) 785–789.
[18] M.D. Halls, J. Velkovski, H.B. Schlegel, Theor. Chem. Acc. 105 (2001) 413–421.
[19] K. Hermann, A. Michalak, M. Witko, Catal. Today 32 (1996) 321–327.
[20] A. Michalak, M. Witko, K. Hermann, Surf. Sci. 375 (1997) 385–394.
[21] A. Chakrabarti, K. Hermann, R. Druzinic, M. Witko, F. Wagner, M. Petersen, Phys. Rev. B 59 (1999) 10583–10590.
[22] K. Hermann, M. Witko, R. Druzinic, Faraday Discuss. 114 (1999) 53–66.
[23] M. Witko, K. Hermann, R. Tokarz, Catal. Today 50 (1999) 553–565.
[24] M. Cavalleri, K. Hermann, A. Knop-Gericke, M. Havecker, R. Herbert, C. Hess, A. Oestereich, J. Dobler, R. Schlogl, J. Catal. 262 (2009) 215–223.
[25] M. Anstrom, N.Y. Topsoe, J.A. Dumesic, J. Catal. 213 (2003) 115–125.
[26] E. Broclawik, A. Gora, M. Najbar, J. Mol. Catal. A 166 (2001) 31–38.
[27] C.D. Wagner, W.M. Riggs, L.E. Davis, J.F. Moulder, G.E. Muilenberg, Handbook of X-ray Photoelectron Spectroscopy, Perkin-Elmer, Minnesota, 1979.
[28] A.E. Lewandowska, M. Calatayud, E. Lozano-Diz, C. Minot, M.A. Banares, Catal. Today 139 (2008) 209–213.